A Parametric Study of Displacement Measurements Using Digital Image Correlation Method

Kuendong Ha*
Technology Division, Samsung Display Devices Co., Ltd.

A detailed and thorough parametric study of digital image correlation method is presented. A theoretical background and development of the method were introduced and the effects of various parameters on the determination of displacement outputs from the raw original and deformed image information were examined. Use of the normalized correlation coefficient, the use of 20 to 40 pixels for a searching window side, 6 variables searching, bi-cubic spline subpixel interpolations and the use of coarse-fine search are some of the key choices among the results of parametric studies. The displacement outputs can be further processed with two dimensional curve fitting for the data noise reduction as well as displacement gradient calculation.

Key Words : Digital Image Correlation Method (DICM), Pattern Matching, Smoothing Technique, Gray Intensity, Bi-Cubic Spline, Normalized Correlation Coefficient, Subimage, Newton-Raphson Method, Homogeneous Deformation

1. Introduction

It is very important in the solid mechanics field to use an accurate and convenient tool for experimental strain analyses, especially for nonlinear behavior of specimens with high strain gradients. Measurements of surface displacements are often used to develop and verify mechanical models under deformation. In fracture mechanics among other topics, some novel experimental techniques have been introduced to determine the strain field around crack tips in validating theoretical constitutive models for use in predicting crack growth.

Among them, the digital image correlation method (DICM) is one of many new experimental methods (Sutton, 1993). This method is one of the surface coating methods in application of photogrammic principles. Grid method uses the same photogrammic principle as that of DICM in a sense that both methods compare two photographs before and after loading to extract the displacement fields, but DICM implements a computer vision instead of manual digitization to get more efficient and accurate results.

Although DICM has been successfully applied by others in a variety of applications, there has not been an in-detail assessment of key parameters in the measured full-field deformations. The effect of the interpolation scheme, the number of bits in the A/D converter and the ratio of frequency of the signal to the frequency of the data sampling has been reported as the most significant parameters (Sutton, 1987). However, the latter two are not controllable parameters under a given experimental set-up. It has been also reported that a larger subimage provides greater accuracy in strain measurements, with little change in resolution of the translation measurements (Sutton, 1988). On the other hand, one requires the use of smallest possible subimage while retaining reasonable accuracy so that the representative strain in the subimage not be smeared out over unnecessarily large subimage area. Also, Knauss

* **E-mail** : kuendong@samsung.co.kr
TEL : +82-331-210-8351 ; **FAX** : +82-331-210-8379
Technology Division, Samsung Display Devices Co., Ltd., Suwon, Korea (Manuscript **Received** July 28, 1999; **Revised** February 14, 2000)

and Vendroux (1994) reported that the use of a least squares coefficient in the image comparison gave almost the same displacement resolution while increasing the computing speed and simplifying the convergence algorithm as compared to the results from the use of the maximum correlation coefficient. To validate these assertions and to find out other key parameters' roles in a practical application for the best displacement results using DICM in a given measuring system, it becomes important and informative to conduct a systemetic parametric study for all the relevant variables during the image preparation to post-processing stages. Another motivation is to provide some help for anyone interested or engaged in DICM application to get better displacement results in a given measuring system. The detailed theory of deformation used for digital image correlation algorithm with sub-pixel interpolation will be briefly introduced before code validation and the experimental parametric investigation.

2. Theoretical Background

2.1 Theory of deformation for use in digital image correlation

Consider an object that is illuminated by a light source and the object is under deformation. Digital image of a body is simply a discrete record of the light intensities present at various positions of the body. A speckle effect, or random dot pattern, as shown at Fig. 1 can be generated by a nonreflective spraying paint on a specimen surface. The undeformed and deformed gray scale images in Fig. 1 reflects the deformation of biaxial strip specimen of inert solid propellant under 5% prescribed strain. For a close look, we can observe the movements of the random patterns in the same direction as the applied strain. A pixel is a basic picture element in a camera sensor, called charge coupled device (CCD) and its value ranges from 0 to 255 when 8 bit A/D convert is employed. Its physical size depends on both camera lens magnification for the focused image and resolution of the CCD sensor. This lens magnification should be constant and the painted surface be well in focus throughout the deformation process to get uniform scale in the digital images.

Let the surface of an object be under planar deformation and $f(x, y)$ and $f^*(x^*, y^*)$ are the gray intensity functions corresponding to surfaces of the undeformed and deformed configurations, respectively. Also let's define a subimage or an image subset to be a set of gray intensity patterns enclosed by thick lines as shown in Fig. 2. If one supposes that the intensity pattern after deformation is related to the initial intensities through the object deformation, then this suggests that there also exists a correlation between the two images to detect the object deformation. That is, if we assume that the paint coating on a surface location sticks to that material position during the deformation, then the gray level on one material point is a unique marking which does not change with deformation. Further we neglect the out-of-plane displacement so that the subimage deformation is approximated by in-plane deformation

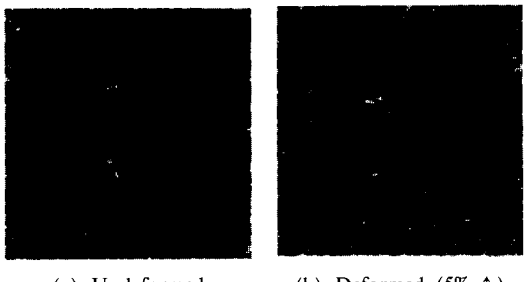

(a) Undeformed (b) Deformed (5% ↕)

Fig. 1 Typical random black and white speckle patterns (250×250 pixels)

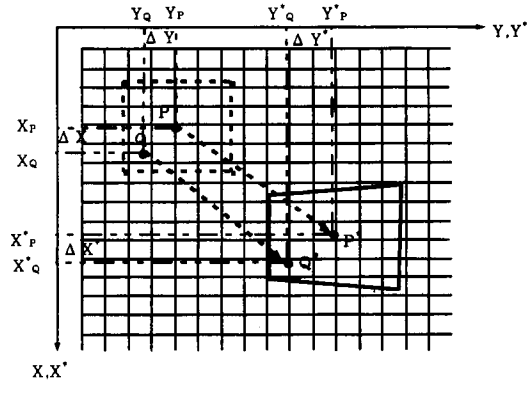

Fig. 2 Deformation of subimage in a sampling grid

and the local deformation within a small subimage is linear in the initial coordinates.

Consider points P and Q in a subimage prior to deformation that are located at positions (x, y) and $(x+dx, y+dy)$ as shown in Fig. 2. After deformation the points P and Q move to P^* and Q^*. Then P^* and Q^* would be traced from P and Q using the linear deformation relations such that,

$$\begin{aligned} f^*(P^*) &= f^*(x+u(P),\ y+v(P)) \\ &= f(P) \\ f^*(Q^*) &= f^*(x+u(Q),\ y+v(Q)) \\ &= f(Q) \end{aligned} \tag{1}$$

From Taylor's expansion of displacement functions $u(x, y)$ and $v(x, y)$ about P up to the first order,

$$\begin{aligned} u(Q) &= u(P) + \left(\frac{\partial u}{\partial x}\right)_P dx + \left(\frac{\partial u}{\partial y}\right)_P dy \\ v(Q) &= v(P) + \left(\frac{\partial v}{\partial x}\right)_P dx + \left(\frac{\partial v}{\partial y}\right)_P dy \end{aligned} \tag{2}$$

Substituting (2) into (1), we have

$$\begin{aligned} f^*(Q^*) = f^*\Big(&x+u(P)+\left(\frac{\partial u}{\partial x}\right)_P dx \\ &+\left(\frac{\partial u}{\partial y}\right)_P dy,\ y+v(P)+\left(\frac{\partial v}{\partial x}\right)_P dx \\ &+\left(\frac{\partial v}{\partial y}\right)_P dy\Big) = f(Q). \end{aligned} \tag{3}$$

The deformed center point in the subimage, P may be found from the gray intensity patterns $f(Q)$ and $f^*(Q^*)$ at the points surrounding P. There are six variables to be determined in Eq. (3), i. e., $u(P)$, $v(P)$, $\left(\frac{\partial u}{\partial x}\right)_P$, $\left(\frac{\partial u}{\partial y}\right)_P$, $\left(\frac{\partial v}{\partial x}\right)_P$, $\left(\frac{\partial u}{\partial y}\right)_P$ from intensity patterns on P^* and Q^* in the deformed image by matching them to those for the positions P and Q in the undeformed image. For each trial set of u_i, v_i, $\left(\frac{\partial u}{\partial x}\right)_i$, $\left(\frac{\partial v}{\partial y}\right)_i$, $\left(\frac{\partial u}{\partial y}\right)_i$ and $\left(\frac{\partial v}{\partial y}\right)_i$ evaluated at P, the searching subimage of intensity patterns are compared to the target subimage in the deformed configuration using a statistical measure of correlation, to represent the pattern-matching quality. Specifically, the normalized least square differences of gray intensities of the two images (Knauss, 1994), summation of absolute differences (Kahn-Jetter, 1989) and normalized correlation coefficient are some of the available statistical measures. The normalized least square error may be defined as

$$E = \sum_i^N \frac{(f_i - f_i^*)^2}{(255 \cdot 255)}, \tag{4}$$

where f_i and f_i^* are the gray scales under undeformed and deformed configurations respectively as defined above, and N denotes the number of sampling points in the subimage. Normalized correlation coefficient is expressed in a discrete form as,

$$C = \frac{\sum_i^N f_i(x, y) * f_i^*(x+\xi, y+\eta)}{\left[\sum_i^N [f_i(x, y)]^2 \sum_i^N [f_i^*(x+\xi, y+\eta)]^2\right]^{1/2}}, \tag{5}$$

where ξ and η are the distance in the x-and y-direction respectively from the center point to its surrounding pixel location in the subimage, defined as follows.

$$\begin{aligned} \xi &= u_i + \left(\frac{\partial u}{\partial x}\right)_i \Delta x + \left(\frac{\partial u}{\partial y}\right)_i \Delta y \\ \eta &= v_i + \left(\frac{\partial v}{\partial x}\right)_i \Delta x + \left(\frac{\partial v}{\partial y}\right)_i \Delta y \end{aligned} \tag{6}$$

A correlation coefficient of $C=1$ indicates a perfect match, $C=0$ means no correlation and $C=-1$ means perfect mismatch.

Subpixel Interpolation : Because the gray scale intensity information is spatially discrete in nature, no gray scale information is available between each pixel position. In the minimization process of the correlation function $S=1-C$, it is not always true for a deformed location, x^* and y^* to be matched to the digitized pixel position exactly. Therefore an approximation of gray level values between each pixel position is needed. Bi-linear interpolation approximates the gray intensity value at a point (x^*, y^*), which is inside a square with four corners of pixel positions at (i, j), $(i+1, j)$, $(i, j+1)$ and $(i+1, j+1)$, by

$$f^* = a_{00} + a_{10} \cdot \Delta x' + a_{01} \cdot \Delta y' + a_{11} \cdot \Delta x' \cdot \Delta y'. \tag{7}$$

Another interpolation method to fit the gray intensity surface data is the use of bi-cubic polynomial interpolation. The functional form of gray scale at (x^*, y^*) is,

$$f^* = a_{00} + a_{10} \cdot \Delta x' + a_{20} \cdot (\Delta x')^2 + a_{30} \cdot (\Delta x')^3 + a_{01} \cdot \Delta y' + a_{02} \cdot (\Delta y')^2 + a_{03} \cdot (\Delta y')^3 + a_{11} \cdot \Delta x' \cdot \Delta y' + a_{21} \cdot (\Delta x')^2 \cdot \Delta y' + a_{31} \cdot (\Delta x')^3 \cdot \Delta y' + a_{12} \cdot (\Delta y')^2 \cdot \Delta x' + a_{22} \cdot (\Delta y')^2 \cdot (\Delta x')^2 + a_{23} \cdot (\Delta y')^2 \cdot (\Delta x')^3 + a_{33} \cdot (\Delta y')^3 \cdot (\Delta x')^3 \quad (8)$$

where $\Delta x'$, $\Delta y' = x$ and y distance from pixel (i, j),

a_{00}=gray intensity level of pixel (i, j), a_{10}= gray intensity level of pixel $(i, j) - a_{00}$, a_{01}=gray intensity level of pixel $(i, j+1) - a_{00}$, a_{11}=gray level of pixel $(i+1, j+1) - a_{00} - a_{10} - a_{01}$ and the remaining a_{ij}'s are determined using the continuation conditions of the first and cross derivatives of f^* at integer pixel locations.

2.2 Verification of the digital image correlation method

To find out the optimum values of 6 variables of the center point in a subimage in Eq. (3), it is necessary to seek the optimization of C or $S=1-C$ by changing all the variables in a sufficiently wide range. To make this process more efficient, so called "coarse-fine" searching method (Sutton, 1986) may be employed. If one can narrow down the searching window range of u, v of the center point to be within 1 or 2 pixels width so that no other local maximum point can be exist, we may use the Newton-Raphson method to locate the center point to the best pattern matching position in the deformed subimage through the value of local maximum coefficient.

A computer program for a series of displacement measurements of many subimage centers was developed to implement this local optimization algorithm by use of digitized image informations before and after the deformation. In order to determine the utility of the proposed method, three sets of experiments were performed. They are : (1) verification of code through image fabrication, (2) translation tests and (3) uniaxial tension tests.

It is very important to check if there are any mistakes in the computer program. The best way of doing so would be to create a image of known movement from the reference subimage of gray intensities (Sutton, 1995). From the random integer array between 0 and 255 for an original image and through the bi-linear interpolation, if the pixel position of deformed subimage falls between integer pixels of the sampling positions, the deformed image can be fabricated. Both translation and linear deformations were applied as if we had ideal experimental conditions between the images before and after the deformation. The images used were 200 by 200 pixels and data sampling for DICM was performed at 9 points (3 columns in a row). The verification test for a deformed image with uniform translations predicted almost exactly the same movement, as the maximum error was less than 0.006 pixel, which corresponds to less than 0.1% deviation from the imposed displacement. The error is purely from the numerical manipulation process in the algorithm including truncation errors in the interpolation process. Note that the synthesized picture was fabricated by using bi-linear interpolation for simplicity, while the DICM scheme uses bi-cubic interpolation. The deviation of the predicted displacements from the imposed displacements are within an acceptable error bound and hence, it is believed that the DICM routine is verified. The higher error in strain implies that the error source may be amplified in strain calculated from displacement due to the differentiation of error (Mostafavi, 1978).

A rigid body translation test is the simplest displacement case that can be measured by the DICM. Rigid body translation tests are frequently used for pin-pointing the displacement error estimation. Positioning errors are reported on the order of 0.1 pixel (Sutton, 1983) for carefully prepared specimen surfaces, low magnifications, and optimum lighting. The rigid body translation experiments and spatial calibrations were performed in the same relatively simple arrangement following Stanglmaier (1993). The test apparatus is shown in Fig. 3. A micrometer with a 0.01 mm resolution was used to displace a commercially available yellow rubber band specimen horizontally across the translation table. Such a calibration is performed by tracking down a target point, since the micrometer indicates the true translation

displacement of the target.

Rigid body translation tests were performed by moving the translation table by a known amount, and the displacements of forty nine points of 7 columns by 7 rows in a image were measured using the DICM, and a statistical analysis was performed. These forty nine points were centered within a small (40 by 40 pixels) subimage of an undeformed image. Figure 4(a) contains the horizontal displacement (u) measurements for an experiment in which a black rubber specimen was displaced by 0.05 mm, which corresponds to 5.35 pixels in horizontal movement and -0.128 pixel in vertical movement (v). The averaged displacement measurements were 5.267 pixels and -0.256 pixel. All horizontal and vertical displacements were within 0.1 pixel of the average, and standard deviations were 0.0028 and 0.0029 pixel, respectively. The results of these rigid body translation tests suggest that conservative positioning error of the DIC method be taken to be within 0.1 pixel. This positioning error is independent of the displacement magnitude because the error is not sensitive to the "offset" of the two comparison images. It is comparable to the accuracy reported by others (Sutton, 1987).

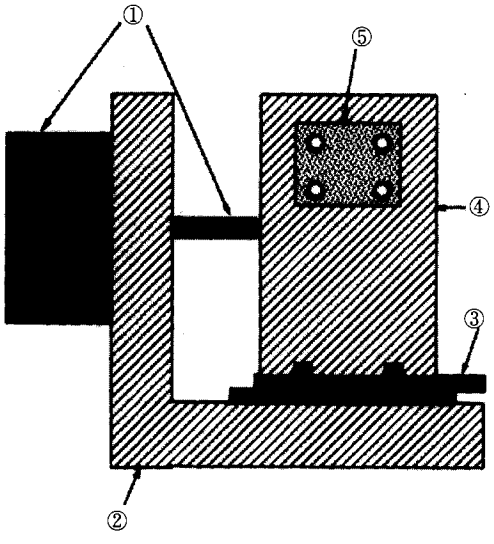

① Micrometer with 0.01 mm Resolution
② Base
③ Translation Table
④ Stand
⑤ Uniaxial Rubberband Specimen

Fig. 3 Apparatus for rigid body translation tests

A strip of commercially available rubber band was cut to a length of 60.0 mm, width of 5.0 mm and thickness of 0.71 mm. The apparatus used was very similar to the one in Fig. 3 used for rigid body translation test, except that one end of the rubber specimen is fixed while the other end is moves together with the micrometer, giving rise to uniform strain in most of the specimen. The specimen gage length was considered to be the total distance between the grips, which held the specimen in place by pressing both ends with a small aluminum plate against its base and the stand. A total of five different "strained" stages were recorded, and measurements were taken at 11~13 data points that were uniformly spaced along the mid line of the rubber strip specimen. Figure 4(b) shows the measured horizontal displacements in which a rubber band specimen was

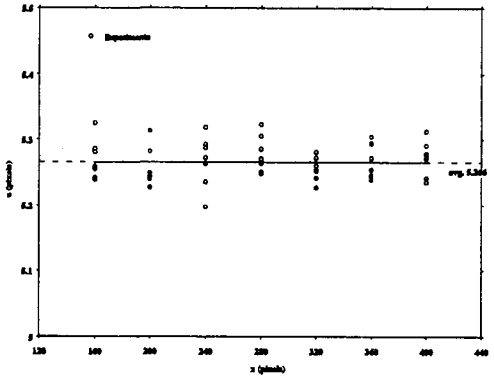

(a) Rigid body translation of black rubber

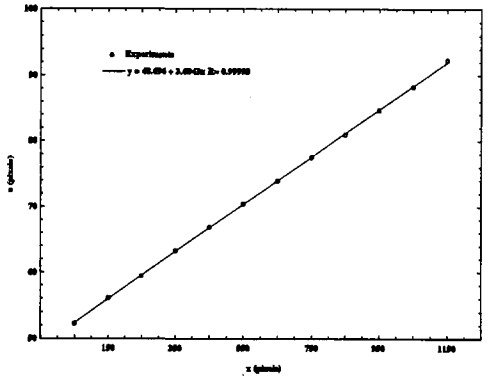

(b) u vs. x (3.6% global strain imposed)

Fig. 4 Typical experimental results for verification of DICM measurements

Table 1 Summary of strain measurements

Stages	Applied Strain (%)	Measured Strain (%)	Difference (%)
2	0.42	0.40	5.0
3	1.48	1.32	3.4
4	2.54	2.51	1.2
5	3.60	3.60	0.0
6	4.66	4.71	1.1

strained to global strains of 3.60%. The linear least square fittings of displacement data are also shown on the plot and the slope is 3.60% of almost uniform horizontal strain, which is very close to the imposed nominal strain. Table 1 shows the comparison between the imposed and measured strains from five different strained images. The experimental measurements are in quite good agreements with the imposed global strains. The maximum error from the expected uniform strain prediction is about 5% for 0.42% global strain, as summarized on Table 1. Noticing how the effect of the positioning displacement error of the DICM decreases with increasing strain levels, the error could be from noise due to small strain signal. It should be pointed out that the noise from displacement data, which could be either from inherent limitations of the DICM or from precision tolerance of the equipment, can be determined and removed from the data without altering the character of the underlying displacement using the so-called 'smoothing technique' (Busby, 1988).

2.3 Determination of displacement and strain field

In many cases, the equipment and techniques have inherent limitations which manifest themselves as noise in the data. When the noise is unknown or noisy data is too ambiguous to interpret, some technique is required to identify and separate the noise from the data. Consequently it is unwise to construct an interpolation function which agrees precisely with the measured displacements at input locations. Particularly if derivatives are sought, it is normally advantageous to formulate a smoothed, approximate representation of the measured values. Least-square algorithms have been used effectively to eliminate the noise from underlying signal.

One technique that is often well-suited for this purpose is the use of spline functions. In our study, Dohrmann and Busby's two dimensional smoothing algorithm (Dohrmann, 1990) was selected. The algorithm uses Wahba's (1975) generalized cross validation (GCV) method to determine the level of noise internally and optimally smooth two dimensional data in a rectangular grid with uniform interval in each direction.

The two dimensional smoothing problem requires finding the bi-cubic spline which minimizes the function φ,

$$\Phi(f)=\sum_{i=1}^{n}\sum_{j=1}^{n}(f(x_i,\ y_i)-z_{ij})^2+\mu\sum_{i=1}^{n}\int_{x_1}^{x_n}\left(\frac{\partial^3 f}{\partial x^3}\right)^2 dx+\mu\sum_{i=1}^{n}\int_{y_1}^{y_n}\left(\frac{\partial^3 f}{\partial y^3}\right)^2 dy+\mu^2\sum_{i=1}^{n}\sum_{j=1}^{n}\int_{x_1}^{x_n}\int_{y_1}^{y_n}\left(\frac{\partial^6 f}{\partial x^3\partial y^3}\right)^2 dxdy \tag{9}$$

where z_{ij} is a set of data at $(x_i,\ y_j)$, μ is a smoothing parameter, f is a bi-cubic spline function and n, $\bar{n}$ are numbers of data in x and y directions, respectively. The displacement function $f(x,\ y)$ can be expressed as a combination of products of basis functions $s_i(x)$ and $\bar{s}_j(y)$ in the x and y directions, such as

$$f(x,\ y)=\sum_{i=1}^{n}\sum_{j=1}^{\bar{n}}c_{ij}s_i(x)\ \bar{s}_j(y) \tag{10}$$

where c_{ij}'s are bi-cubic spline coefficients and $s_i(x)$, $\bar{s}_j(y)$ are expressed in terms of polynomials upto third order in x and y, respectively (Ha, 1996). For example, the basis functions $s_i(x)$ are polynomials such as,

$$\begin{aligned} s_1(x)&=1\\ s_2(x)&=(x-x_1)\\ s_3(x)&=(x-x_1)^2\\ s_{i+1}(x)&=\begin{cases}0 & \text{for } x<x_i\\ (x-x_i)^3/6 & \text{for } x_i\le x<x_{i+1}\\ h^3/6+h^2(x-x_{i+1})+h(x-x_{i+1})^2/2 & \text{for } x_i\ge x,\end{cases}\end{aligned} \tag{11}$$

and $\bar{s}_j(y)$ is defined similarly as Eq. (11) in terms of y and j instead of x and i, respectively.

The bi-cubic spline displacement function f and its derivatives $\frac{\partial^{(k+l)}f}{\partial x^k \partial y^l}$ $(k, l=1, 2)$ are continuous over the entire rectangular grid because basis functions and their derivatives up to second order are continuous. The value of the smoothing parameter μ can greatly affect the result. If it is too big, the third derivatives of f is forced to vanish, resulting in a two dimensional least square bi-cubic fit. Choosing μ too small gives unsatisfactory roughness, especially in derivatives.

Once the smoothed displacement field is determined in the form of two dimensional cubic spline functions, as given in Eq. (10), the smoothed displacement outputs are assumed free of experimental noise. Then the strain outputs are directly available from their differentiations with respect to x and y when the small strain measure is used, that is

$$\varepsilon_x=\frac{\partial u}{\partial x},\ \varepsilon_y=\frac{\partial v}{\partial y},\ \gamma_{xy}=\left(\frac{\partial v}{\partial x}+\frac{\partial u}{\partial y}\right). \quad (12)$$

From whole field strain data, part of columns or rows data may be extracted for the area of interest and overlaid for further post-processing.

3. Experimental Parameter Study

The undeformed and deformed images of the biaxial specimen of inert solid propellant under 7% global strain focused on the left side edge were tried for the parameter study. The material consists of 70% volume of hard particles with varying sizes (10~100 μm) embedded in a soft rubber binder. Here a solid propellant specimen was selected because this material shows large strains and rotations around its rigid particles which in turn is suitable for providing tough measuring situation to DICM so that the effect of each parameter on DICM performance can be more pronounce. A schematic of the set-up is shown in Fig. 5. It is important that the camera lens plane in front of the specimen be parallel to the specimen surface and the surface mid-line be aligned spatially with a horizontal line to prevent any focusing problem. The displacement field in the test at all the data points ranged from 20 pixels to 85 pixels in the vertical movement and 35 pixels to 87 pixels in the horizontal movement with 100 pixels/mm scale factor. The effect of subimage window size, the effect of sub-pixel interpolation scheme and the effect of number of variables in the matching process are studied over 837 data points. The comparisons for each item were made based on the normalized correlation coefficient and the standard deviations of displacements. Table 2 summarizes this study.

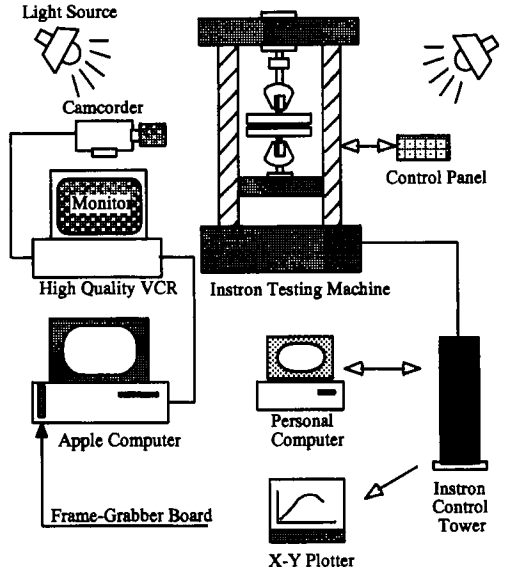

Fig. 5 Test set-up for high accuracy image system

Table 2 Results of parameter study

# Variables	n=2				n=6			
Int. Scheme	Bi-Linear		Bi-Cubic		B I -Linear		Bi-Cubic	
subset szie	20×20	50×50	20×20	50×50	20×20	50×50	20×20	50×50
Average C	0.87	0.83	0.90	0.82	0.917	0.92	0.93	0.90
σ	0.114	0.063	0.072	0.063	0.057	0.047	0.057	0.048

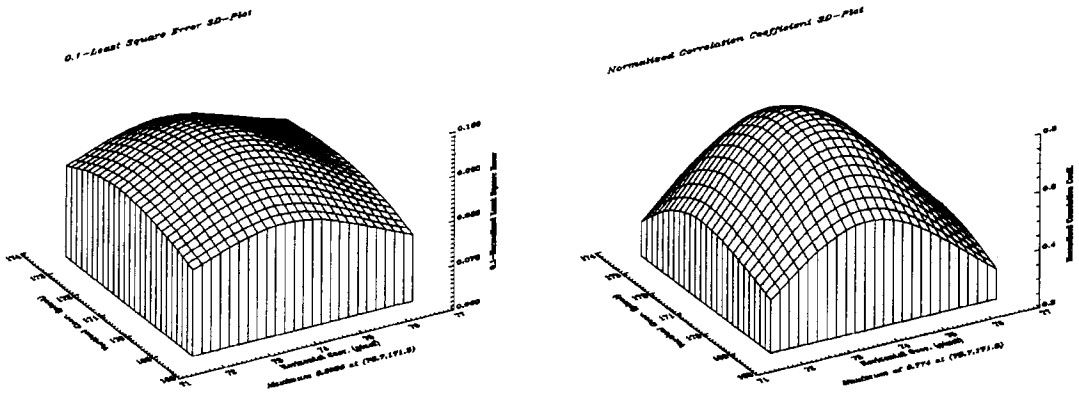

(a) Normalized least square difference (b) Normalized correlation coefficient

Fig. 6 Surface plot comparison of pattern matching measures around maximum point

The effect of subimage window size : The 20 by 20 pixels subimage window size resulted in higher correlation coefficient, higher standard deviation than those from 50 by 50 subimage window as given in Table 2. This can be explained by the fact the standard deviation is higher because there is less pixel data points in the 20 by 20 subimage window than those in the 50 by 50 window and the coefficient is higher because it is easier to match the deformed subimage of smaller size than that of a bigger size. In a separate test, 4 by 4 pixels subimage was used for the second search in subpixel restoration after the initial search. The results were not particularly better than those with the window size from 20 to 50 pixels on a side. The window size from 20 pixels to 50 pixels in each side showed very close agreement with each other. As a summary, even though the differences are small, 20 by 20 window gives locally more accurate matching point. On the other hand, this will make it easier for the DICM results to be contaminated by experimental noise in the data or a false image registration, if any.

The choice of subimage pattern matching measure : The use of least square error in Eq. (4) as a criterion for the best image matching was tried several times in a few preliminary tests. Figure 6(a) and (b) show three dimensional plots of (0.1 — least square error) and normalized correlation coefficient around the local maximum point. Here the height at each pixel coordinate means the measure of how well the searching subimage matches to the target subimage with its center at that position. As shown in the figure, both criteria indicate the displacement of the searching subimage center for the best image-matching condition at (73.7, 171. 9). The correlation coefficient in Fig. 6(b) shows slightly sharper concave upward surface around the local maximum point than the least square error in Fig. 6(a). For example, (0.1 — least square error) value on (72,169) position corresponds to about 81.0% of the maximum value while for normalized correlation coefficient case, it is about 45.2% of the maximum value. Each surface slope to local maximum at the same position of searching subimage more or less signifies better pattern-matching quality in the convergence rate and accuracy of the final displacement of the searching subimage center. In a very few cases, this minor disadvantage of least square measure caused additional problems to the searching subimage such as, oscillations around the local maximum or even passing by the local maximum location. Therefore, to avoid any possibilitiys on convergence problem and to get the maximum accuracy, the use of normalized correlation coefficient is the best choice for DICM. This hypothesis is supported by the author's numerous personal experiences (Ha, 1996) as well as addressed by other researchers, e. g., Tian and Huhns (1983).

Searching algorithm with six variables or two

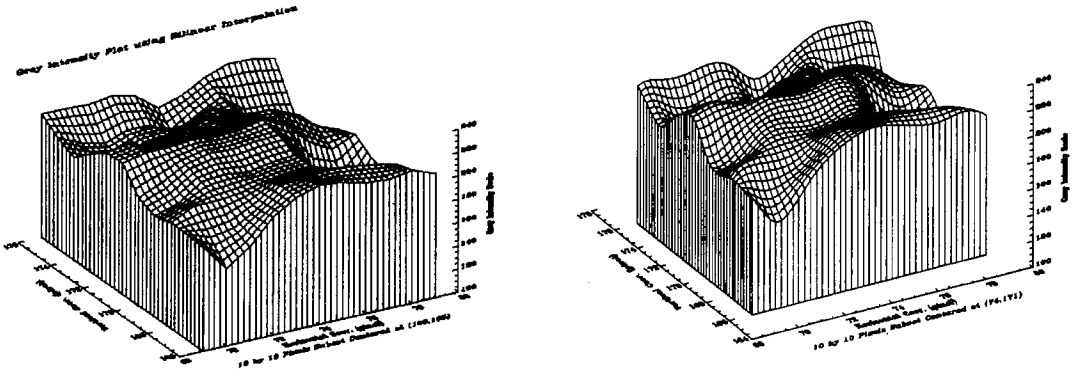

(a) with bi-linear interpolation (b) With bi-cubic spline interpolation

Fig. 7 Light Intensity Surfaces with Interpolation

variables : The linear deformation theory in searching and matching intensity patterns in the DICM algorithm supposedly gives the optimum six variables regarding center point P in Fig. 2 of the deformed subimage, i. e., $u(P)$, $v(P)$, $\left(\frac{\partial u}{\partial x}\right)_P$, $\left(\frac{\partial u}{\partial y}\right)_P$, $\left(\frac{\partial v}{\partial x}\right)_P$, $\left(\frac{\partial u}{\partial y}\right)_P$. Inasmuch as the latter four gradient terms do not directly contribute to the displacement determination process which functions as the fine-tuning terms for the primary varaiables, u and v in Eq. (2), these four variables sometimes manifested themselves in non-physical erroneous values. It is checked if these erroneous gradient terms may work against locating accurate displacements by trying searching with and without these four gradient terms. After comparing the results for both cases of n=2 and n=6 as shown in Tables 2, it was found that the searching algorithm with six variables resulted in higher correlation coefficient and more consistant correlations (smaller standard deviation on C) than the case of searching with two variables. This means that these four variables are not directly connected into the subimage deformation, but they work more mathematically for better correlation value after primary positioning of the subimage governed by u and v. Nevertheless, the effect of the number of variables is not considered to be a critical one, provided fine search is performed after initial the coarse search to confine the searching area, especially for the cases of searching with smaller subimage window size, e. g., 10 by 10 pixels.

The effect of interpolation scheme : Bi-linear and bi-cubic interpolation scheme as defined in Eq. (7) and Eq. (8) were compared for the sub-pixel interpolation scheme. The examples of three dimensional images interpolated as such are shown in Fig. 7. As we may notice in the figure, the one from bi-cubic interpolation scheme in Fig. 7(a) looks much smoother and more natural than the one from bi-linear interpolation. The performance comparison of the two is also given in Table 2. For the averaged normalized correlation coefficient value with almost the same standard deviation, bi-cubic interpolation scheme gives a clear advantage over the bi-linear interpolation scheme.

The effect of Rigid Body Rotation : Raw data images should be compensated for the rotation of the aluminum pulling grips before the image-matching analyses using DICM. The rotation of the grips in the process of specimen deformation can be monitored from the LVDT's secured in the holes near the edges of the grips, as shown in Fig. 5. To compensate for the skewed image due to an initial camera rotation in the optical set-up, the original image should be rotated back so that they are well aligned with a spatial horizontal line. After the separation of possible image misalignment, a grip rotation due to the nonuniform deformation can be compensated for the elimination of rigid body rotation. For a simple compensation example of grip rotation, refer to Ha (1996). Figure 8(a) shows a typical result of the grip rotation for the biaxial strip specimen of

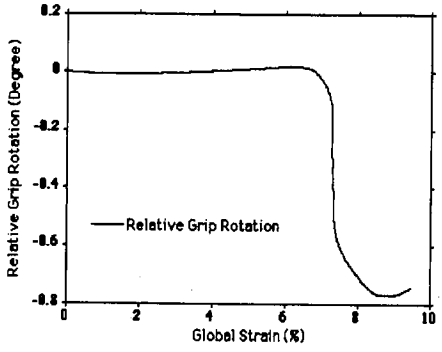

(a) Relative grip rotation of biaxial specimen

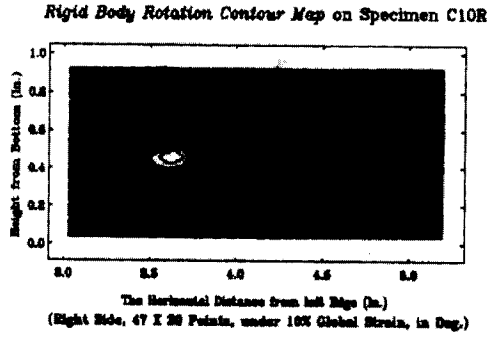

(b) Rigid body rotation angle around crack tip

Fig. 8 Separation and Monitoring of Rigid Body Rotation Components

inert solid propellant. In the figure, the maximum rotation is less than 0.06°. This specimen typically failed just before the large grip rotation began as indicated in Fig. 8(a). The wake region behind the crack-lip line usually underwent some rigid body rotation as the crack growth continued and its angle is overlaid on the picture of crack tip in Fig. 8(b). The rigid body rotation angle, θ was calculated through the use of Lagrangian strain tensor ε^L and Polar Decomposition Theorem; when we denote F and C as in-plane deformation tensor and right Cauchy-Green tensor, defined as $F=(1+\nabla u)$, $C=F^TF$ respectively, the rigid body rotation part of the deformation process, Q can be computed from,

$$Q=F(\sqrt{C})^{-1}=\begin{pmatrix}\cos\theta & -\sin\theta\\ \sin\theta & \cos\theta\end{pmatrix}. \qquad (13)$$

For the safe side as Knauss (1994) pointed out, it would be best to use finite strain measurement allowing for large rotations.

The effect of image equalization : It is very important to prepare the raw images with high contrast and good focus. In that sense, it seems very plausible that to maximize the contrast of the raw images, some of image processing skills may be used to improve the contrast between the pixels of the lowest to highest gray scale in the image. An equalizing process in image processing is a way to enhance the contrast of a gray scaled image by extrapolating the range of the gray scale employed in the original image into the maximum range of 0 to 255 gray scale. From the analysis, the image looks better after equalization, but it does not give any better displacement or strain contour map than those from the original images.

The effect of removing erroneous data : It was observed that in a few cases, there were obvious local displacement errors from the initial data sources, e. g. blurred images, big spots of the same light intensity and similar gray patterns among others. Usually the number of points was not significant, at most two or three points, even though in most cases there were no such bad data outputs at all. Using the surface fitting scheme, those points were eliminated before the displacement fittings for strain calculations and interpolated by surrounding data points. The comparison with and without this scheme revealed this correction process helped a bit locally when correlation coefficient of less than 0.8 were used for the criterion of the bad data selection.

The effect of out-of-plane displacement : The influence of out-of-plane displacement, w on in-plane strain ε_y, for example, can be assessed from finite strain magnitude, i. e. from the Lagrangian strain, ε_y^L. Let u, v be the in-plane displacements in the x and y-direction respectively. Then

$$\varepsilon_y^L=\left[1+2\frac{\partial v}{\partial y}+\left(\frac{\partial u}{\partial y}\right)^2+\left(\frac{\partial v}{\partial y}\right)^2+\left(\frac{\partial w}{\partial y}\right)^2\right]^{1/2}-1. \qquad (14)$$

From Eq. (14), it should be assured that the term $\left(\frac{\partial w}{\partial y}\right)^2$ is negligible in comparison to $2\frac{\partial v}{\partial y}$

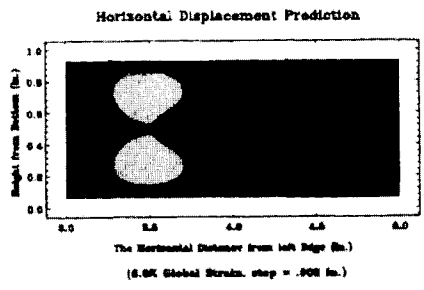

(a) Horizontal displacement contour map

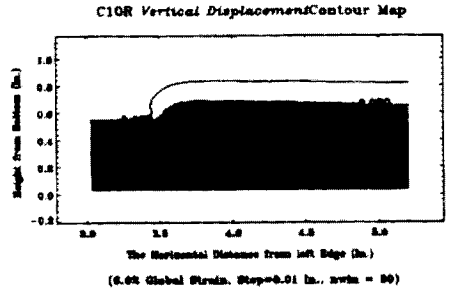

(b) Vertical displacement contour map

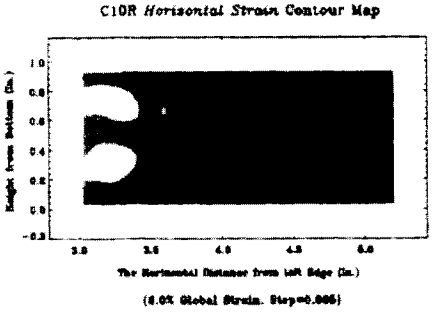

(c) Horizontal strain contour map

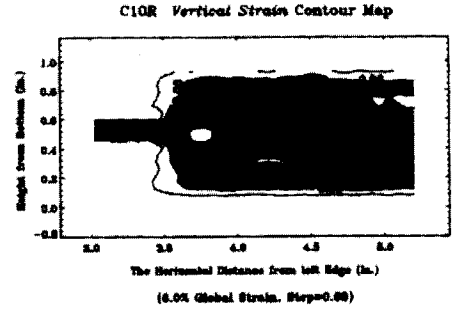

(d) Vertical strain conteour map

Fig. 9 Surface contour maps in the right side of specimen with a central crack

to get rid of the influence of w. If w is found to be insignificant in the calculation of in-plane strains as was the case for the given material (Post, 1987), then the influence of w in DICM algorithm is also negligible.

It should be noted that each item of the above parametric studies is an independent process which could be considered separately without affecting the conditions of other parameters. Some of the items in the above parametric studies are related to post-processing skills and initial enhancement of original digital images. Other variables, such as number of variables and subimage size in the search algorithm are independent with each other. Therefore it is assumed that there is no coupling effect between the parameters.

In most of other experimental applications, bi-cubic interpolation, window size of 30 to 40 pixels a side, six variables searching, normalized correlation coefficient were selected and used. Any rigid body rotations due to the initial camera misalignment was compensated by rotating back before running DICM computer codes. In a highly deformed area like crack tip region and near the crack lips, false matching results were reported in a few points. The change of subimage window size, usually to a smaller one, change of the searching point to a very near neighborhood and replacement of bad points with interpolated ones with surrounding data solved these bad correlation cases. Figure 9 illustrates typical examples of horizontal and vertical surface displacement and strain fields determined from the DICM with the optimal parameters decided using the method described above for a bi-axial specimen with a central thru-crack under 5% global strain.

4. Conclusions

Surface deformation measurement skill called Digital Image Correlation Method is described and verified through image fabrication, rigid body translation and uniaxial tension tests. The estimates of errors are found to be within 0.1 pixel from the inherent test method limitation. Through

parametric study for the effects of all the possible variables, including the subimage size, the image-matching criterion, the number of variables and sub-pixel interpolation scheme on the performance of DICM were conducted using a uniaxial tension test. The use of six variables for searching subimage, with 30 to 40 pixels of a subimage in a side and bi-cubic spline subpixel interpolation method and maximum correlation coefficient are best suited for the best displacement results. In determination of strain field, it is recommended to use bigger subimage for displacement curve fitting to get smooth strain field and smaller subimage for local correction of abnormal strain field. The displacement fields are to be processed by smoothing technique for noise reduction and strain field calculations.

References

Bruck, H. A., McNeil, S. R., Sutton, M. A. and Peters III, W. H., 1989, "Digital Image Correlation Using Newton-Raphson Method of Partial Differential Correlation," *Experimental Mechanics*, Vol. 29, No. 5, pp. 261~267.

Busby, H. R. and Dohrmann, C. R., 1988, "Algorithms for Smoothing Noisy Data with Spline Functions and Smoothing Parameter Selection," *Proc. VI Int. Cong. on Exp. Mech.*, Vol. II, pp. 843~849.

Dohrmann, C. R. and Busby, H. R., 1990, "Spline Function Smoothing and Differentiation of Noisy Data on a Rectangular Grid," *Proc. 1990 SEM Spring Conf. on Exp. Mech.*, pp. 76~84.

Ha, K., 1996, "Evaluation of A Three-Dimensional, Viscoelastic Constitutive Model of Solid Propellant with Distributed Damage," *Ph. D. Dissertation, The University of Texas*, pp. 193~195.

Kahn-Jetter, Z. L. and Chu, T. C., 1990, "Three-Dimensional Displacement Measurements Using Digital Image Correlation and Photogrammic Analysis," *Experimental Mechanics*, Vol. 30, No. 2, pp. 10~16.

Post, D., Smith, C. W. and Czarnek, R., 1987, "Crack Opening and Extension in Inert Solid Propellant," *Final Report No. AFRL TR-87-043* prepared for AFAL, VPI&SU, pp. 20~23.

Pulos, G. C. and Knauss, M. G., 1993, "High Resolution Crack Length Measurements through Computer Vision," *Novel Experimental Techniques in Fracture Mechanics*, ASME AMD-Vol. 176, pp, 185~201.

Sutton, M. A., Cheng, Minggi, Peters, W. H. Chao, Y. J. and Mcneil, S. R., 1986, "Application of an Optimized Digital Correlation Method to Planar Deformation Analysis," *Image and Vision Computing*, Vol. 4, No. 3, pp. 143~150.

Sutton, M. A., McNeil, S. R., Jang, J. and Babai, M, 1987, "Effect of Subpixel Image Restoration on Digital Image Correlation Error Estimates," *Optical Engineering*, Vol. 27, No. 10, pp. 870~877.

Sutton, M. A., Chao, Y. and Lyons, J. S., 1993, "Computer Vision Methods for Surface Deformation Measurements in Fracture Mechanics," *Novel Experimental Techniques in Fracture Mechanics*, ASME AMD-Vol. 176, pp. 203~217.

Sutton, M. A., 1995, in private communications.

Stanglmaier, R. H., 1993, "Strain and Displacement Measurement by Cross-Correlating Digital Images," *EMRL Report No. 93/4*, University of Texas at Austin, pp. 21~28.

Tian, Q. and Huhns, M. N., 1983, "A Fast Hill Climbing Algorithm for Measuring Object Displacement with Sub-Pixel Accuracy," *IEEE 12th Workshop on Applied Imagery Pattern Recognition*, College Park, MD.

Vendroux, G., and Knauss, W. G., 1994, "Deformation Measurements at the Sub-Micron Size Scale: II. Refinements in the Algorithm for Digital Image Correlation," *SM Report 94-5*, California Institute of Technology.

Wahba, G., 1975, "Smoothing Noisy Data with Spline Functions," *Numer. Math.*, Vol. 24, pp. 383~393.